Nanoscopic Morphologies in Block Copolymer Nanorods as Templates for Atomic-Layer Deposition of Semiconductors

By *Yong Wang,* Yong Qin, Andreas Berger, Eric Yau, Changcheng He, Lianbing Zhang, Ulrich Gösele, Mato Knez,* and *Martin Steinhart**

Block copolymers (BCPs) self-assemble into ordered arrays of nanoscopic domains, the nature of which depends on the constituents of the BCPs and their molecular architecture.[1] BCPs have been exploited as precursors for nanoporous materials[2] and as templates for the rational design of nanoscopic architectures with periods from below 10 nm up to the 100-nm-range in thin-film configurations.[3] Whereas molds containing arrays of aligned cylindrical nanochannels with hard confining walls, such as self-ordered anodic aluminum oxide (AAO),[4] have been used to fabricate one-dimensional nanostructures from a plethora of materials,[5] the self-assembly of BCPs in cylindrical confinement has only recently emerged as an access to nanorods exhibiting ordered nanoscopic fine structures.[6] Sol–gels containing precursors for inorganic scaffold materials and BCPs as structure-directing soft templates were infiltrated into AAO. Subsequent gelation and calcination yielded nanorods consisting of various inorganic oxides and amorphous carbon exhibiting ordered mesoporous fine structures.[7] However, direct infiltration of microphase-separated BCP melts into AAO[8] has received much less attention, mainly because of a lack of obvious applications of the solid BCP nanorods thus obtained. Only recently, BCP nanorods have been converted into mesoporous polymeric nanorods by degrading sacrificial blocks[9] and by selective swelling.[10]

BCPs confined to AAO with pore diameters about one order of magnitude larger than their characteristic bulk periods have been reported to retain bulk-like morphologies, such as cylinders oriented along the pore axes and concentric-cylindrical lamellae. Nanoscopic domain structures substantially different from those obtained in the absence of geometric constraints form if BCPs self-assemble within cylindrical pores having diameters of the same order of magnitude than their characteristic periods.[11–13] Wu et al. synthesized silica nanorods containing helical and circular-cylindrical ''stacked-doughnuts'' mesopore structures by gelation and calcination of sol–gels containing poly(ethylene oxide)-*block*-poly(propylene oxide)-*block*-poly(ethylene oxide) and tetraethyl orthosilicate infiltrated into AAO with pore diameters below 70 nm,[11] and prepared metal replicas of helical mesopores by electrochemical deposition.[14] However, only little effort has been directed to the experimental study of BCP melts self-assembling under strong cylindrical confinement,[12] even though the formation of a broad variety of unprecedented confinement-induced nanoscopic domain structures has been predicted.[15] Thus, only a small range of the potentially accessible morphologies has been realized, and their exploitation for the generation of functional nanostructures has not yet been addressed.

Here, we report the fabrication of hierarchical one-dimensional semiconductor nanostructures containing structural motifs, such as helices and stacked doughnuts, that mimic unconventional, confinement-induced nanoscopic domain structures of BCP melts self-assembled in cylindrical nanopores of AAO with appropriate pore diameters. Asymmetric polystyrene-*block*-poly(2-vinylpyridine) (PS-*b*-P2VP; M_n (PS) = 50 000 g mol^{-1}; M_n (P2VP) = 16 500 g mol^{-1}) was infiltrated into AAO, the PS-*b*-P2VP nanorods thus obtained were released (Fig. 1), and the nanoscopic domains consisting of the minority component P2VP were converted to internal mesopores by selective swelling (Fig. 2). The mesoporous PS-*b*-P2VP nanorods were then employed as templates for atomic-layer deposition (ALD) of zinc oxide (ZnO, Figs. 3 and 4), a wide-band-gap II–VI semiconductor that has attracted considerable interest as a potential emitter of blue and UV light.[16]

To describe the morphologies occurring in PS-*b*-P2VP nanorods formed in AAO, we will use the reduced nanorod diameter D/L_0, where D is the absolute diameter of the nanorods and L_0 the center-to-center distance between the P2VP cylinders in the bulk. However, the D/L_0 ratios given below should be considered as estimations rather than as accurate values. Infiltration of asymmetric PS-*b*-P2VP into AAO is accompanied by preferential segregation of the minority component P2VP to the hydroxyl-terminated pore walls, which is possibly mediated by the formation of hydrogen bonds between the nitrogen atoms of the pyridyl moieties and the hydroxyl groups.[10] In case of pore diameters larger than $\approx$ 170 nm ($D/L_0 > 4.0$), away from the AAO/BCP interface a bulk-like morphology characterized by

[*] Dr. Y. Wang, Prof. M. Steinhart, Dr. Y. Qin, Dr. A. Berger, E. Yau, L. Zhang, Prof. U. Gösele, Dr. M. Knez
Max Planck Institute of Microstructure Physics
Weinberg 2, 06120 Halle/Saale (Germany)
E-mail: steinhart@mpi-halle.de
Dr. Y. Wang
State Key Laboratory of Materials-Oriented Chemical Engineering
Nanjing University of Technology
Nanjing 210009, Jiangsu (P. R. China)
E-mail: Yongwang@njut.edu.cn
Prof. M. Steinhart
Intitute for Chemistry
University of Osnabrück
Barbarastraße 7
D-49069 Osnabrück
Dr. C. He
Department of Chemistry
Beijing Normal University
Beijing, 100875 (P. R. China)

DOI: 10.1002/adma.200900136

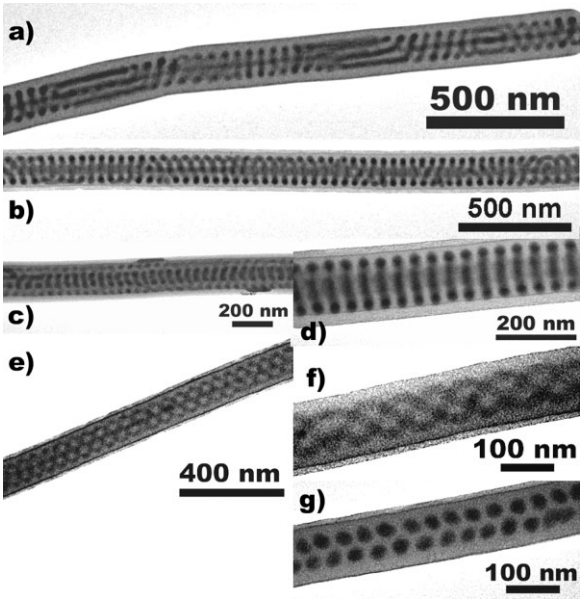

Figure 1. TEM images of native PS-*b*-P2VP nanorods released from AAO with pore diameters ranging from ≈170 down to ≈100 nm. The P2VP domains were selectively stained with I_2 and appear darker than the PS matrix. a) $D \approx 170$ nm, $D/L_0 \approx 4.0$; b)–d) $D \approx 150$ nm, $D/L_0 \approx 3.5$; e) $D \approx 133$ nm, $D/L_0 \approx 3.1$; f) $D \approx 119$ nm, $D/L_0 \approx 2.8$; g) $D \approx 104$ nm, $D/L_0 \approx 2.4$.

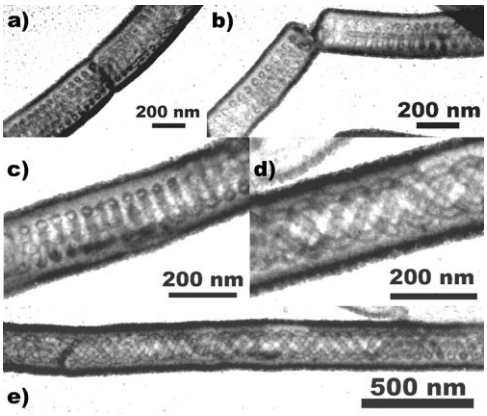

Figure 3. TEM images of mesporous PS-*b*-P2VP nanorods after ALD deposition of ZnO. Owing to its higher mass/thickness contrast, ZnO appears darker than PS and P2VP. A ZnO layer ≈30 nm thick covering the outer surface of the PS-*b*-P2VP nanorods and a ZnO layer ≈10 nm thick covering the walls of the internal mesopores can be clearly identified. a–c) PS-*b*-P2VP nanorods with internal mesopore structures derived from morphologies characterized by P2VP helices and circular-cylindrical P2VP domains (stacked doughnuts) with a pitch or spacing of ≈43 nm. d,e) PS-*b*-P2VP nanorods containing internal mesopores derived from morphologies characterized by multiple P2VP helices with pitches larger than the diameter of the nanorods.

cylindrical P2VP domains oriented along the nanorod axes with a center-to-center distance of ≈43 nm clearly dominates.[10] However, a screening of PS-*b*-P2VP nanorods formed in pores with diameters ranging from 100 to 170 nm, corresponding to D/L_0 values lying between 2.3 and 4, reveals the occurrence of a rich variety of complex, confinement-induced morphologies, the exhaustive discussion of which is beyond the scope of this work. While we could not unambiguously identify a clear D/L_0 threshold value separating ''confinement-induced'' and ''bulk-like'' morphologies, the predominance of the latter for $D/L_0 > 4$ is in line with theoretical predictions.[15] Figure 1 displays some confinement-induced morphologies we have identified. Three morphology types were found in a PS-*b*-P2VP nanorod with $D \approx 170$ nm corresponding to $D/L_0 \approx 4.0$ (Fig. 1a): i) three parallel dark lines representing cylindrical P2VP domains oriented along the nanorod axis; ii) a single P2VP helix winding about a central cylindrical P2VP domain coinciding with the nanorod axis; and iii) stacked-doughnuts structures consisting of circular P2VP cylinders that wind about a central cylindrical P2VP domain coinciding with the nanorod axis. The P2VP doughnuts are oriented perpendicularly to or inclined with respect to the nanorod axis. PS-*b*-P2VP nanorods with $D \approx 150$ nm ($D/L_0 \approx 3.5$)

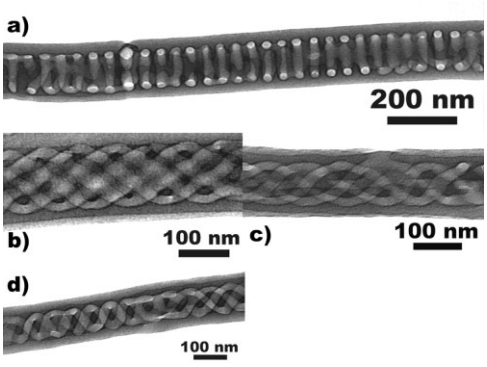

Figure 2. TEM images of mesoporous PS-*b*-P2VP nanorods obtained by selective swelling of the P2VP domains and collapse of the P2VP blocks upon evaporation to the swelling agent. a) Internal mesopores derived from morphologies characterized by P2VP helices and circular-cylindrical P2VP domains (stacked doughnuts) with a pitch or spacing of ≈43 nm, which is clearly smaller than the diameter of the nanorods. b–d) Internal mesopores derived from morphologies characterized by multiple P2VP helices with pitches larger than the diameter of the nanorods.

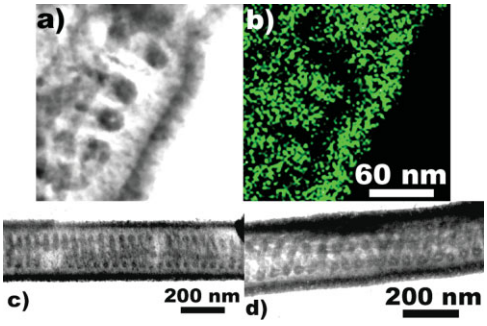

Figure 4. TEM characterization of one-dimensional ZnO nanostructures with hierarchical architecture, which were obtained by ALD using mesoporous PS-*b*-P2VP nanorods as templates and subsequent extraction of the PS-*b*-P2VP with DMF. a) Scanning TEM image of a detail (extraction of the PS-*b*-P2VP with DMF for three days). The outer ZnO shell was damaged so that tubular ZnO replicas of the internal mesopores of the PS-*b*-P2VP nanorods were uncovered. b) EDX mapping of the relative spatial distribution of Zn in the area displayed in a). c,d) TEM images of ZnO nanostructures after extraction of the PS-*b*-P2VP for 14 h. Note the displacement of the central cylindrical entities.

consist of segments containing either stacked P2VP doughnuts or P2VP single helices winding about a continuous central cylindrical P2VP domain coinciding with the nanorod axis (Fig. 1b). Moreover, stacks of circular-cylindrical P2VP domains that surround a second set of discrete disk-shaped or doughnut-shaped P2VP domains located in the middle of the nanorods occur (Fig. 1c and d). The pitch of the P2VP single helices and the spacing between the circular-cylindrical P2VP doughnuts is approximately 43 nm. This value is clearly smaller than the diameter of the nanorods but corresponds to the spacing between the bulk-like P2VP cylinders oriented along the nanorods formed in AAO with pore diameters larger than 180 nm.[10] The nanorod segments with uniform morphology have lengths of the order of a few 100 nm. Apparently, stacked doughnuts oriented normal to the nanorods axis, stacked doughnuts tilted with respect to the nanorod axis, and single helices with similar pitch or spacing can coexist. This finding is in line with theoretical predictions.[15b]

A distinctively different morphology type that apparently emerges when the pore diameter of the AAO is further decreased is characterized by multiple P2VP helices. The single helices have a pitch of $\approx$ 160 nm, thus exceeding the diameters of the PS-*b*-P2VP nanorods. For a D value of 133 nm ($D/L_0 \approx 3.1$), a P2VP triple helix winding about a continuous cylindrical P2VP domain oriented along the nanorod axis was found (Figure 1e). The central cylindrical P2VP domain vanishes if D is reduced to 119 nm ($D/L_0 \approx 2.8$) (Figure 1f). Eventually, the helical structure breaks up to form discrete, distorted P2VP domains upon further decrease of D to 104 nm ($D/L_0 \approx 2.4$) (Figure 1g).

As shown previously,[10] bulk-like cylindrical P2VP domains in PS-*b*-P2VP nanorods can be converted to cylindrical mesopores with walls consisting of P2VP by selective swelling of the P2VP with ethanol. The glassy PS matrix undergoes reconstruction processes to accommodate the increased volume of the swollen P2VP domains and retains its altered shape when the swollen P2VP domains collapse upon drying. However, the moderate P2VP swelling ratio attainable with ethanol as swelling agent is not sufficient to break up the PS matrix, and the initial morphology type of the BCP nanorods is conserved. In this way, we could transform the complex, confinement-induced morphologies of PS-*b*-P2VP nanorods as those displayed in Figure 1 into internal mesopore structures with diameters ranging from 20 to 25 nm mimicking the morphology of the P2VP domains (Fig. 2).

ALD involves successively performed deposition cycles comprising the exposure of the substrates to be coated to the vapors of at least two different precursors. At first, a (sub)monolayer of a reactive precursor species is formed on the substrate, and residual precursor molecules are removed by purging. Subsequently, a second precursor converts the first one into the target compound. The overall thickness of the deposited layer can be adjusted by the number of successive deposition cycles. We exploited the internal mesopore structures in ethanol-treated PS-*b*-P2VP nanorods derived from confinement-induced nanoscopic domain structures as templates for low-temperature ZnO ALD at 60 °C using $Zn(C_2H_5)_2$ and deionized water as precursors, thus adapting a process previously applied to inorganic substrates.[17] Whereas external contours of three-dimensional organic substrates,[18] such as polymeric nanowires,[19,20] plant viruses,[21] and holographically defined three-dimensional polymeric templates,[22] were replicated by ALD of titania and alumina, the ALD process reported here involves the coating of internal surfaces not directly exposed to the ambiance. The mesoscopic polymeric scaffold surrounding the internal mesopores of the PS-*b*-P2VP nanorods is permeable to the ALD precursors, so that even the walls of discrete internal cavities can be coated. However, consistent with previous studies on the permeability of alumina layers deposited by ALD on smooth polymer films,[23] we assume that the ZnO layer deposited onto the outer surface of the PS-*b*-P2VP nanorods increasingly impedes further transport of ALD precursors to the inner walls of the internal mesopores as its thickness increases. Hence, after 200 ALD cycles, a ZnO layer about 10 nm thick was obtained on the walls of the internal mesopores, which is significantly thinner than the ZnO layer about 30 nm thick on the outer surface of the PS-*b*-P2VP nanorods (Fig. 3). The tubular nature of the helical and circular-cylindrical ZnO entities thus fabricated is obvious from Figure 3b and c. Their diameters range from 25 to 30 nm, and appear to be slightly larger than those of the mesopores in the swollen PS-*b*-P2VP nanorods, indicating the presence of an interfacial layer with a thickness of a few nm in which coordination of the nitrogen atom of the pyridyl groups of the P2VP repeat units to the Zn possibly plays a role.

Extraction of the PS-*b*-P2VP with dimethylformamide yields one-dimensional ZnO nanostructures characterized by hierarchical architectures, which consist of outer ZnO shells encasing tubular ZnO helices and stacked doughnuts as well as straight ZnO tubes. Uncovered tubular ZnO replicas of the internal mesopores of a PS-*b*-P2VP nanorod located in a ZnO nanostructure with damaged outer ZnO shell (Fig. 4a) unambiguously contain Zn, since they can clearly be identified in the mapping of the relative spatial distribution of Zn by means of energy-dispersive X-ray (EDX) spectroscopy (Fig. 4b). The position of the unsupported internal ZnO entities is no longer fixated by a supporting BCP matrix, so that they are, to some extent, displaced (Fig. 4c and d).

In conclusion, PS-*b*-P2VP nanorods with confinement-induced morphologies substantially different from their bulk counterparts were prepared within cylindrical nanopores of self-ordered AAO. The nanoscopic morphologies thus obtained comprised domains of the minority component P2VP characterized by helical structure motifs and stacked doughnuts that were converted to internal mesopore structures by selective swelling of the P2VP with ethanol. The mesoporous PS-*b*-P2VP nanorods thus obtained were used as templates for ALD of ZnO, which involved diffusion of the precursors through the polymeric scaffold and deposition of ZnO on the walls of the internal mesopores even if they are discrete cavities. Hence, ZnO nanostructures characterized by hierarchical architectures that contain hollow helices and stacked doughnuts mimicking the confinement-induced nanoscopic domain structures of the block-copolymer nanorods were obtained. Using one-dimensional and zero-dimensional[24] BCP nanostructures exhibiting internal nanoscopic domain structures as templates for ALD should be a generic method for the fabrication of novel nanostructures consisting of a broad range of target materials that exhibit complex morphologies. The synthesis of helical nanostructures can be considered as the starting point for the design of chiral separation media, catalyst supports, or three-dimensional metamaterials.[25]

Experimental

Self-ordered AAO with a pore diameter of 180 nm and a pore depth of 100 μm was prepared by electrochemical anodization [4b]. An Al_2O_3 layer with a nominal thickness of 40 nm was deposited onto the pore walls by ALD [26] involving 400 cycles of alternating exposure to $Al(CH_3)_3$ and deionized H_2O at a process temperature of 150 °C using a commercial hot-wall flow-type ALD reactor (SUNALE™ R75, Picosun, Finland) operated with N_2 as a precursor carrier and purge gas at a pressure of 10 Pa. The pulse and purge times for both precursors were 0.1 s and 4 s, respectively. Under the same conditions, the deposition rate of Al_2O_3 on a smooth silicon wafer amounted to about 0.95 Å per cycle. The AAO was attached to an underlying aluminum substrate so that the pore bottoms were closed. As a result, the deposited alumina layer was not uniform along the pores. Thus, their actual diameter varied from ≈100 nm at the pore mouths to ≈180 nm near the pore bottoms so that they can be considered as a library imposing different degrees of confinement on infiltrated BCPs.

PS-*b*-P2VP (M_n (PS) = 50 000 g mol^{-1}; M_n (P2VP) = 16 500 g mol^{-1}; M_w/M_n(PS-*b*-P2VP) = 1.09; obtained from Polymer Source Inc., Canada) was infiltrated into ALD-treated AAO at 230 °C for 24 h while a load of approximately 0.7 kg cm^{-2} was applied to accelerate infiltration [27]. Residual PS-*b*-P2VP was then removed from the surface of the AAO with sharp blades. To release the PS-*b*-P2VP nanorods thus formed, the AAO was dissolved at room temperature in 40 wt% aqueous KOH solution within 20 min. Subsequently, three washing steps involving centrifugation, removal of the supernatant solution, and redispersion in deionized water, another washing step with 40 wt% aqueous KOH solution, and three more washing steps with deionized water were performed to obtain neutral aqueous suspensions of the native PS-*b*-P2VP nanorods. Some drops of the suspension were deposited onto copper grids coated with a holey carbon film and exposed to iodine vapor at 60 °C for 30 min to selectively stain the P2VP domains for transmission electron microscopy (TEM) characterization [10,28].

For the selective swelling of the P2VP, 0.2 mL of the aqueous suspensions of the PS-*b*-P2VP nanorods were mixed with 0.8 mL ethanol and heated to 60 °C for 10 min. The swollen PS-*b*-P2VP nanorods were transferred onto copper grids coated with a holey carbon film. Using a commercial hot-wall flow-type ALD reactor (SUNALE™ R75, Picosun, Finland) operated with N_2 as a precursor carrier and purge gas at a pressure of 10 Pa, 200 cycles of ZnO deposition corresponding to a nominal layer thickness of 30 nm were carried out at 60 °C with $Zn(C_2H_5)_2$ and deionized water as precursors. Pulse and purge times of 0.2 s and 5 s were applied for $Zn(C_2H_5)_2$, and of 2 s and 5 s for H_2O, respectively.

The TEM images seen in Figures 1–3, 4c and d were taken using a JEOL 1010 microscope operated at 100 keV. The relative spatial distribution of Zn displayed in Figure 4b was obtained by mapping the intensities of the Zn Kα peak at 8.64 keV using a Philips CM20 FEG microscope operated at 200 KeV. The corresponding TEM image seen in Figure 4a was taken in the scanning transmission electron microscopy mode.

Acknowledgements

This work was funded by the German Research Foundation (Priority Program 1165 ''Nanowires and Nanotubes'', STE 1127/6) and the German Ministry of Education and Research (project no. 03X5507). Technical support by S. Kallaus and K. Sklarek is gratefully acknowledged. Y. W. thanks the Alexander von Humboldt Foundation for a fellowship.

Received: January 13, 2009
Revised: February 13, 2009
Published online: April 14, 2009

[1] a) F. S. Bates, G. H. Fredrickson, *Annu. Rev. Phys. Chem.* **1990**, *41*, 525. b) V. Abetz, P. F. W. Simon, *Adv. Polym. Sci.* **2005**, *189*, 125.
[2] M. A. Hillmyer, *Adv. Polym. Sci.* **2005**, *190*, 137.
[3] a) M. Park, C. Harrison, P. M. Chaikin, R. A. Register, D. H. Adamson, *Science* **1997**, *276*, 1401. b) T. Thurn-Albrecht, J. Schotter, G. A. Kästle, N. Emley, T. Shibauchi, L. Krusin-Elbaum, K. Guarini, C. T. Black, M. T. Tuominen, T. P. Russell, *Science* **2000**, *290*, 2126.
[4] a) H. Masuda, F. Fukuda, *Science* **1995**, *268*, 1466. b) H. Masuda, K. Yada, A. Osaka, *Jpn. Y. Appl. Phys. Part 2-Lett.* **1998**, *37*, L1340.
[5] C. R. Martin, *Science* **1994**, *266*, **1961**.
[6] M. Steinhart, *Adv. Polym. Sci.* **2008**, *220*, 123.
[7] a) Z. Yang, Z. Niu, X. Cao, Z. Yang, Y. Lu, Z. Hu, C. C. Han, *Angew. Chem. Int. Ed.* **2003**, *42*, 4201. b) Q. Lu, F. Gao, S. Komarneni, M. Chan, T. E. Mallouk, *J. Am. Chem. Soc.* **2004**, *126*, 8650. c) M. Steinhart, C.-D. Liang, G. W. Lynn, U. Gösele, S. Dai, *Chem. Mater.* **2007**, *19*, 2383.
[8] a) H. Q. Xiang, K. Shin, T. Kim, S. I. Moon, T. J. McCarthy, T. P. Russell, *Macromolecules* **2004**, *37*, 5660. b) Y. Sun, M. Steinhart, D. Zschech, R. Adhikari, G. H. Michler, U. Gösele, *Macromol. Rapid Commun.* **2005**, *26*, 369. c) J. D. Sievert, *Ph.D. Thesis*, Amherst **2006**.
[9] Y. Wang, U. Gösele, M. Steinhart, *Chem. Mater.* **2008**, *20*, 379.
[10] Y. Wang, U. Gösele, M. Steinhart, *Nano Lett.* **2008**, *8*, 3548.
[11] Y. Wu, G. Cheng, K. Katsov, S. W. Sides, J. Wang, J. Tang, G. H. Fredrickson, M. Moskovits, G. D. Stucky, *Nat. Mater.* **2004**, *3*, 816.
[12] a) K. Shin, H. Q. Xiang, S. I. Moon, T. Kim, T. J. McCarthy, T. P. Russell, *Science* **2004**, *306*, 76. b) H. Xiang, K. Shin, T. Kim, S. I. Moon, T. J. McCarthy, T. P. Russell, *Macromolecules* **2005**, *38*, 1055. c) H. Xiang, K. Shin, T. Kim, S. Moon, T. J. McCarthy, T. P. Russell, *J. Polym. Sci. Part B* **2005**, *43*, 3377.
[13] X. Chen, M. Knez, A. Berger, K. Nielsch, U. Gösele, M. Steinhart, *Angew. Chem. Int. Ed.* **2007**, *46*, 6829.
[14] Y. Wu, T. Livneh, Y. X. Zhang, G. Cheng, J. Wang, J. Tang, M. Moskovits, G. D. Stucky, *Nano Lett.* **2004**, *4*, 2337.
[15] See, for example: a) B. Yu, P. Sun, T. Chen, Q. Jin, D. Ding, B. Li, *Phys. Rev. Lett.* **2006**, *96*, 138306. b) B. Yu, Q. Jin, D. Ding, B. Li, A.-C. Shi, *Macromolecules* **2008**, *41*, 4042.
[16] M. H. Huang, S. Mao, H. Feick, H. Yan, Y. Wu, H. Kind, E. Weber, R. Russo, P. Yang, *Science* **2001**, *292*, 1897.
[17] E. Guziewicz, I. A. Kowalik, M. Godlewski, K. Kopalko, V. Osinniy, A. Wójcik, S. Yatsunenko, E. Łusakowska, W. Paszkowicz, M. Guziewicz, *J. Appl. Phys.* **2008**, *103*, 033515.
[18] M. Knez, K. Nielsch, L. Niinistö, *Adv. Mater.* **2007**, *19*, 3425.
[19] R. H. A. Ras, M. Kemell, J. de Wit, M. Ritala, G. ten Brinke, M. Leskelä, O. Ikkala, *Adv. Mater.* **2007**, *19*, 102.
[20] a) M. Kemell, V. Pore, M. Ritala, M. Leskela, M. Linden, *J. Am. Chem. Soc.* **2005**, *127*, 14178. b) Q. Peng, X.-Y. Sun, J. C. Spagnola, G. K. Hyde, R. J. Spontak, Gregory, N. Parsons, *Nano Lett.* **2007**, *7*, 719. c) G. M. Kim, S. M. Lee, G. H. Michler, H. Roggendorf, U. Gösele, M. Knez, *Chem. Mater.* **2008**, *20*, 3085.
[21] M. Knez, A. Kadri, C. Wege, U. Gösele, H. Jeske, K. Nielsch, *Nano Lett.* **2006**, *6*, 1172.
[22] J. S. King, E. Graugnard, O. M. Roche, D. N. Sharp, J. Scrimgeour, R. G. Denning, A. J. Turberfield, C. J. Summers, *Adv. Mater.* **2006**, *18*, 1561.
[23] M. D. Groner, S. M. George, R. S. McLean, P. F. Carcia, *Appl. Phys. Lett.* **2006**, *88*, 051907.
[24] T. Higuchi, A. Tajima, K. Motoyoshi, H. Yabu, M. Shimomura, *Angew. Chem. Int. Ed.* **2008**, *47*, 8044.
[25] J. B. Pendry, *Science* **2004**, *306*, 1353.
[26] R. L. Puurunen, *J. Appl. Phys.* **2005**, *97*, 121301.
[27] O. Kriha, L. Zhao, E. Pippel, U. Gösele, R. B. Wehrspohn, J. H. Wendorff, M. Steinhart, A. Greiner, *Adv. Funct. Mater.* **2007**, *17*, 1327.
[28] J. J. Chiu, B. J. Kim, E. J. Kramer, D. J. Pine, *J. Am. Chem. Soc.* **2005**, *127*, 5036.